IEEE Access
Multidisciplinary ⋮ Rapid Review ⋮ Open Access Journal

Received 13 July 2023, accepted 24 August 2023, date of publication 1 September 2023, date of current version 21 September 2023.

Digital Object Identifier 10.1109/ACCESS.2023.3311350

RESEARCH ARTICLE

Robustness Analysis of a Fixed-Time Convergent GNN for Online Solving Sylvester Equation and Its Application to Robot Path Tracking

ZHIGUO TAN AND ZHENLUN YANG
School of Information Engineering, Guangzhou Panyu Polytechnic, Guangzhou 511483, China

Corresponding author: Zhiguo Tan (tanzhiguo136@163.com)

This work was supported in part by the Guangdong Innovative Projects with Characteristics in Colleges and Universities under Grant 2022KTSCX292, in part by the Scientific Research Project of Guangzhou Panyu Polytechnic under Grant 2022KJ03, and in part by the Guangzhou Municipal Science and Technology Bureau of China under Grant 202002030133.

ABSTRACT It is shown in a recently published work that the GNN (gradient-based neural network) model activated by the msbp (modified sign-bi-power) function exhibits superior fixed-time convergence for solving the Sylvester equation in the noise-free case. Encouraged by this point, in this paper, we study its robust performance when it is disturbed by three kinds of noises, i.e., dynamic bounded vanishing noise, dynamic bounded non-vanishing noise, and constant noise. Detailed mathematical analyses are conducted to show the robustness properties (e.g., convergence property, the upper bound of steady-state solution error) of the GNN model, which are further verified by two simulation examples. Ultimately, the GNN model is applied to the path tracking of a planar four-link redundant robot arm.

INDEX TERMS Gradient-based neural network, Sylvester equation, robustness analysis, robot path tracking.

I. INTRODUCTION

In the domain of scientific research and engineering, a considerable number of applications [1], [2], [3], [4], [5], [6], such as observer design, state estimation, commutative rings, and pole placement, are germane to the solution to the Sylvester equation. Mathematically, the Sylvester equation to be investigated can be formulated as the following form [6]:

$$CX(t) - X(t)D + F = 0 \in \mathbb{R}^{m\times n}, \tag{1}$$

where C and D are respectively m-dimensional and n-dimensional square matrices, F is an $m\times n$ rectangle matrix, and $X(t)$ is used to stand for the unknown $m \times n$ matrix variable that needs to find out. Because of its wide application background, solving the Sylvester equation is of monumental significance and has been widely concerned [7], [8], [9], [10].

Generally, two types of solving schemes are available for the Sylvester equation [6]. One is the classical numerical algorithms with diverse forms, e.g., the Bartels-Stewart algorithm [11], skew-Hermitian splitting iteration algorithm [12], iterative algorithms based on gradient [13], [14]. Due to the intrinsic property of serial computing, numerical algorithms may be short of competitiveness and efficiency for the situation where a real-time calculation is required, and the coefficient matrices involved are of large dimension [15], [16]. The other is the parallel-processing schemes, e.g., recurrent neural networks (RNNs). In comparison to numerical algorithms, RNNs, which have been applied to robot motion planning [17], [18], [19], [20], [21], [22], time-varying linear system [23], nonlinear control [24], are more appropriate and provide a puissant alternative for large-scale and/or real-time computation due to their two intrinsic characteristics: parallel-processing and hardware implementability [5], [25], [26].

Gradient-based neural network (GNN) and zeroing neural network (ZNN) are two typical representatives of RNNs [25], [26]. For GNN and ZNN, offline training is not required, while their convergence can be guaranteed in theory [27].

The associate editor coordinating the review of this manuscript and approving it for publication was Amjad Ali.

This feature, together with the aforementioned two intrinsic characteristics, renders GNN and ZNN to be potent computing tools that can be applied to diverse scenarios. As for the Sylvester equation solving, many ZNN models were proposed. An integration-enhanced ZNN model activated by nonlinear function was proposed in [9]. In [5], a ZNN model with an exponential time-varying parameter was designed. In [2], to solve the complex-valued Sylvester equation, a complex-valued ZNN model was established. These ZNN models all take advantage of the derivative information of the time-varying coefficients and can tackle the time-varying Sylvester equation at the cost of a relatively complex structure. On the other hand, some GNN models that ignore the derivative information and thus have a simple structure were proposed to solve the static Sylvester equation. A linear GNN model with global exponential convergence was investigated in [15]. Note that exponential convergence belongs to infinite-time convergence, and finite-time convergence is more favorable. To achieve this goal, a GNN model that takes the sbp (sign-bi-power) function as its activation function was proposed in [28]. Along with the deep-going of the research, it is found that finite-time RNNs (including GNNs) may also be short of competitiveness and efficiency for some real-time applications that need to meet strict time limits [29] due to the fact that their convergence times are dependent of the initial value of the neural states. To get around this issue, a fixed-time convergent GNN model that takes the modified sbp (msbp) function as its activation function was thus proposed in [26], which is formulated as follows:

$$\begin{aligned}\dot{X}(t) = &-\eta C^{\mathrm{T}}\Psi_{\mathrm{msbp}}(CX(t) - X(t)D + F) \\ &+ \eta\Psi_{\mathrm{msbp}}(CX(t) - X(t)D + F)D^{\mathrm{T}}, \end{aligned} \tag{2}$$

where scalar parameter $\eta > 0$ is germane to the convergence time, and $\Psi_{\mathrm{msbp}}(\cdot) \in \mathbb{R}^{m\times n}$ is called the activation function array with its every element being the function $\psi_{\mathrm{msbp}}(\cdot)$ defined as

$$\psi_{\mathrm{msbp}}(x) = a|x|^{\mu}\mathrm{sign}(x) + bx + c|x|^{\nu}\mathrm{sign}(x). \tag{3}$$

Herein, $a, b, c > 0$, $0 < \mu < 1$, and $\nu > 1$.

In comparison to the GNN models presented in [15] and [28], it is found that the GNN model (2) without taking any noises into account can attain superior fixed-time convergence [26]. It's important to note that noises (including external perturbation and model realization errors) exist inevitably in real problems [30]. As a consequence, it is desirable and of important implications to investigate the robust performance of the GNN model (2). In view of this, the main focus of this work is the noise-polluted GNN model (2) formulated as follows:

$$\begin{aligned}\dot{X}(t) = &-\eta C^{\mathrm{T}}\Psi_{\mathrm{msbp}}(CX(t) - X(t)D + F) \\ &+ \eta\Psi_{\mathrm{msbp}}(CX(t) - X(t)D + F)D^{\mathrm{T}} + R(t), \end{aligned} \tag{4}$$

where $R(t) \in \mathbb{R}^{m\times n}$ could be a time-variant or constant bounded noise.

The main contributions and novelties of this study are stated as follows.

1) The robust performance against three kinds of noises of the recently-presented msbp-function-activated GNN model (4) for solving the Sylvester equation is studied.
2) Theoretical analyses show that if disturbed by a dynamic bounded vanishing noise, the GNN model (4) can still achieve fixed-time convergence, and if disturbed by a dynamic bounded non-vanishing or constant noise, an SSSE (steady-state solution error) exists and has a bound.
3) The convergence time of fixed-time convergence, the SSSE bound, and the finite time and exponential convergence rate for the solution error approaching the bound are also estimated.
4) Two simulative examples are conducted to verify the theoretical analysis. In addition, the GNN model (4) is successfully applied to the path tracking of a planar four-link redundant robot arm.

The rest of this paper is structured as follows. In Section II, the robustness of the GNN model (4) in the presence of three types of noises is theoretically investigated. In Section III, Two simulation examples are provided to verify the theoretical results. In Section IV, a path-tracking example of a planar four-link redundant robot arm, is provided to show the feasibility and efficacy of the GNN model (4) to robotic applications. Finally, some remarks are given in Section V.

II. ROBUSTNESS ANALYSIS

In this section, the robustness of the GNN model (4) in the presence of three kinds of noises (i.e., dynamic bounded vanishing noise, dynamic bounded non-vanishing noise, and constant noise) is theoretically investigated. For clarity, it is assumed that the Sylvester equation (1) admits a unique solution. Before presenting the main results, the following lemma is offered to facilitate the subsequent analysis.

Lemma 1 [31], [32]: If $0 < \rho \leq 1$ and $\varrho > 1$, then

$$\sum_{i=1}^{K}\zeta_i^{\rho} \geq \left(\sum_{k=1}^{K}\zeta_i\right)^{\rho}, \sum_{i=1}^{K}\zeta_i^{\varrho} \geq K^{1-\varrho}\left(\sum_{i=1}^{K}\zeta_i\right)^{\varrho},$$

are satisfied for non-negative numbers $\zeta_i, i = 1, 2, \ldots, K$.

A. DYNAMIC BOUNDED VANISHING NOISE

When $R(t)$ is a dynamic bounded vanishing noise, we have the following theoretical result regards the convergence of the GNN model (4).

Theorem 1: For the Sylvester equation (1) with the unique theoretical solution X^*, if GNN model (4) is disturbed by a dynamic bounded vanishing noise $R(t)$ satisfying $|r_{ij}(t)| \leq \epsilon|\varepsilon_{ij}(t)|$, where $r_{ij}(t)$, $\varepsilon_{ij}(t)$ are separately the ijth elements of $R(t)$ and matrix $X(t) - X^*$, and $\epsilon > 0$ is a constant. Then, under arbitrary initial condition $X(0)$, the neural variable $X(t)$ of the GNN model (4) with $\lambda\eta b \geq \epsilon$ attains fixed-time

convergence, and the upper bound of convergence time:

$$T_{\max} = \frac{2}{\eta a(2\lambda)^{\frac{1+\mu}{2}}(1-\mu)} + \frac{2(mn)^{\frac{\nu-1}{2}}}{\eta c(2\lambda)^{\frac{1+\nu}{2}}(\nu-1)}, \tag{5}$$

where $\lambda > 0$ denotes the minimal eigenvalue of $P^{\mathrm{T}}P$ with matrix P defined later.

Proof: For the convenience of expression, let $X^* \in \mathbb{R}^{m\times n}$ indicate the theoretical solution of the Sylvester equation (1), and two vector variables are defined, i.e., $\boldsymbol{w}(t) := \mathrm{vec}(X(t)) \in \mathbb{R}^{mn}$ and $\tilde{\boldsymbol{w}}(t) := \boldsymbol{w}(t) - \mathbf{w}^*$, where $\mathbf{w}^* := \mathrm{vec}(X^*) \in \mathbb{R}^{mn}$ and $\mathrm{vec}(\cdot)$ is the vectorization operator [33], [34]. In view of the property of the Kronecker product $\otimes$: $\mathrm{vec}(AXB) = (B^{\mathrm{T}} \otimes A)\mathrm{vec}(X)$, the following equivalent vector-form of the matrix-form GNN model (4) is handily gained.

$$\begin{aligned}
\dot{\tilde{\boldsymbol{w}}}(t) &= \dot{\boldsymbol{w}}(t)\\
&= -\eta(I_n \otimes C^{\mathrm{T}} - D \otimes I_m)\mathrm{vec}(\Psi_{\mathrm{msbp}}(CX(t) - X(t)D\\
&\quad + F)) + \mathrm{vec}(R(t))\\
&= -\eta(I_n \otimes C^{\mathrm{T}} - D \otimes I_m)\Psi^{\mathrm{v}}_{\mathrm{msbp}}(\mathrm{vec}(CX(t) - X(t)D\\
&\quad + F)) + \boldsymbol{r}(t)\\
&= -\eta P^{\mathrm{T}}\Psi^{\mathrm{v}}_{\mathrm{msbp}}((I_n \otimes C - D^{\mathrm{T}} \otimes I_m)(\boldsymbol{w}(t) - \mathbf{w}^*)) + \boldsymbol{r}(t)\\
&= -\eta P^{\mathrm{T}}\Psi^{\mathrm{v}}_{\mathrm{msbp}}(P\tilde{\boldsymbol{w}}(t)) + \boldsymbol{r}(t),
\end{aligned} \tag{6}$$

where I_n stands for the n-by-n unit matrix, $\Psi^{\mathrm{v}}_{\mathrm{msbp}}(\cdot) = \mathrm{vec}(\Psi_{\mathrm{msbp}}(\cdot)) \in \mathbb{R}^{mn}$, $\boldsymbol{r}(t) = \mathrm{vec}(R(t))$, and matrix $P := I_n \otimes C - D^{\mathrm{T}} \otimes I_m$.

In view of (6), a Lyapunov function based on Euclid-norm $\|\cdot\|_2$ is defined as $\varpi(t) = \|\tilde{\boldsymbol{w}}(t)\|_2^2/2$ [26], [33]. The conclusions that $\varpi(t)$ is of positive definiteness and $\varpi(t) \to +\infty$ provided $\tilde{\boldsymbol{w}}(t) \to \infty$ are clear. Now, we are going to compute the time derivative of $\varpi(t)$ as follows:

$$\begin{aligned}
\dot{\varpi}(t) &= \tilde{\boldsymbol{w}}^{\mathrm{T}}(t)\dot{\tilde{\boldsymbol{w}}}(t)\\
&= -\eta(P\tilde{\boldsymbol{w}}(t))^{\mathrm{T}}\Psi^{\mathrm{v}}_{\mathrm{msbp}}(P\tilde{\boldsymbol{w}}(t)) + \tilde{\boldsymbol{w}}^{\mathrm{T}}(t)\cdot\boldsymbol{r}(t)\\
&= \sum_{i=1}^{mn}\Big(-\eta a(|[P\tilde{\boldsymbol{w}}(t)]_i|^2)^{\frac{1+\mu}{2}} - \eta b|[P\tilde{\boldsymbol{w}}(t)]_i|^2\\
&\quad - \eta c(|[P\tilde{\boldsymbol{w}}(t)]_i|^2)^{\frac{1+\nu}{2}}\Big) + \sum_{i=1}^{mn}[\tilde{\boldsymbol{w}}(t)]_i \cdot r_i(t)\\
&\le -\eta a(\sum_{i=1}^{mn}|[P\tilde{\boldsymbol{w}}(t)]_i|^2)^{\frac{1+\mu}{2}} - \eta b\sum_{i=1}^{mn}|[P\tilde{\boldsymbol{w}}(t)]_i|^2\\
&\quad - \eta c(mn)^{\frac{1-\nu}{2}}(\sum_{i=1}^{mn}|[P\tilde{\boldsymbol{w}}(t)]_i|^2)^{\frac{1+\nu}{2}}\\
&\quad + \sum_{i=1}^{mn}|[\tilde{\boldsymbol{w}}(t)]_i|\cdot\epsilon|[\tilde{\boldsymbol{w}}(t)]_i|\\
&= -\eta a(\tilde{\boldsymbol{w}}^{\mathrm{T}}(t)P^{\mathrm{T}}P\tilde{\boldsymbol{w}}(t))^{\frac{1+\mu}{2}} - \eta b(\tilde{\boldsymbol{w}}^{\mathrm{T}}(t)P^{\mathrm{T}}P\tilde{\boldsymbol{w}}(t))\\
&\quad - \eta c(mn)^{\frac{1-\nu}{2}}(\tilde{\boldsymbol{w}}^{\mathrm{T}}(t)P^{\mathrm{T}}P\tilde{\boldsymbol{w}}(t))^{\frac{1+\nu}{2}} + 2\epsilon\varpi(t)\\
&\le -\eta a(2\lambda)^{\frac{1+\mu}{2}}\varpi^{\frac{1+\mu}{2}}(t) - 2(\lambda\eta b - \epsilon)\varpi(t)\\
&\quad - \eta c(mn)^{\frac{1-\nu}{2}}(2\lambda)^{\frac{1+\nu}{2}}\varpi^{\frac{1+\nu}{2}}(t)\\
&\le -\eta a(2\lambda)^{\frac{1+\mu}{2}}\varpi^{\frac{1+\mu}{2}}(t) - \eta c(mn)^{\frac{1-\nu}{2}}(2\lambda)^{\frac{1+\nu}{2}}\varpi^{\frac{1+\nu}{2}}(t)\\
&= -k_1\varpi^{\frac{1+\mu}{2}}(t) - k_2\varpi^{\frac{1+\nu}{2}}(t)\\
&\le 0,
\end{aligned} \tag{7}$$

where $\lambda > 0$ is the minimal eigenvalue of the real symmetric matrix $P^{\mathrm{T}}P$, $k_1 = \eta a(2\lambda)^{\frac{1+\mu}{2}}$, and $k_2 = \eta c(mn)^{\frac{1-\nu}{2}}(2\lambda)^{\frac{1+\nu}{2}}$. Therefore, according to Lemma 2 of [33], $\tilde{\boldsymbol{w}}(t)$ is fixed-time convergent to the equilibrium point $\tilde{\boldsymbol{w}}(t) = \mathbf{0}$. This fact, together with $\tilde{\boldsymbol{w}}(t) = \boldsymbol{w}(t) - \mathbf{w}^* = \mathrm{vec}(X(t) - X^*)$, demonstrates that neural state $X(t)$ is fixed-time convergent to the exact solution X^* of the Sylvester equation (1). Moreover, according to Lemma 2 of [33], the upper bound of fixed-time convergence is estimated as

$$\begin{aligned}
T_{\max} &= \frac{1}{k_1(1-\frac{1+\mu}{2})} + \frac{1}{k_2(\frac{1+\nu}{2}-1)}\\
&= \frac{2}{\eta a(2\lambda)^{\frac{1+\mu}{2}}(1-\mu)} + \frac{2(mn)^{\frac{\nu-1}{2}}}{\eta c(2\lambda)^{\frac{1+\nu}{2}}(\nu-1)},
\end{aligned}$$

which completes the proof. ■

Remark 1: A similar result is obtained by ZNN (Theorem 2 of [7]). The main difference between them is that $T_{\max}$ obtained by ZNN model in [7] is irrelevant to the eigenvalue of matrix $P^{\mathrm{T}}P$.

B. DYNAMIC BOUNDED NON-VANISHING NOISE

When $R(t)$ is a dynamic bounded non-vanishing noise, we have the following result regards the steady-state solution error (SSSE) bound of the GNN model (4).

Theorem 2: For the Sylvester equation (1) with the unique theoretical solution X^*, if GNN model (4) is disturbed by a dynamic bounded non-vanishing noise $R(t)$ satisfying $\|R(t)\|_{\mathrm{F}} \le \sigma$ with $\sigma > 0$ being a constant. Then, under arbitrary initial condition $X(0)$, the SSSE of the GNN model (4) is given as

$$\lim_{t\to+\infty}\|X(t) - X^*\|_{\mathrm{F}} < \Big(\frac{\sigma}{\eta a\lambda^{\frac{1+\mu}{2}}}\Big)^{1/\mu}, \tag{8}$$

where $\lambda > 0$ denotes the minimal eigenvalue of $P^{\mathrm{T}}P$ with P defined the same as that in Theorem 1. It follows from (8) that the SSSE approaches 0 as $\eta a \to +\infty$.

Proof: It follow from (7) that

$$\begin{aligned}
\dot{\varpi}(t) &= \tilde{\boldsymbol{w}}^{\mathrm{T}}(t)\dot{\tilde{\boldsymbol{w}}}(t)\\
&= -\eta(P\tilde{\boldsymbol{w}}(t))^{\mathrm{T}}\Psi^{\mathrm{v}}_{\mathrm{msbp}}(P\tilde{\boldsymbol{w}}(t)) + \tilde{\boldsymbol{w}}^{\mathrm{T}}(t)\cdot\boldsymbol{r}(t)\\
&\le -\eta a(\sum_{i=1}^{mn}|[P\tilde{\boldsymbol{w}}(t)]_i|^2)^{\frac{1+\mu}{2}} - \eta b\sum_{i=1}^{mn}|[P\tilde{\boldsymbol{w}}(t)]_i|^2\\
&\quad - \eta c(mn)^{\frac{1-\nu}{2}}(\sum_{i=1}^{mn}|[P\tilde{\boldsymbol{w}}(t)]_i|^2)^{\frac{1+\nu}{2}} + \|\tilde{\boldsymbol{w}}(t)\|_2\cdot\sigma\\
&= -\eta a(\tilde{\boldsymbol{w}}^{\mathrm{T}}(t)P^{\mathrm{T}}P\tilde{\boldsymbol{w}}(t))^{\frac{1+\mu}{2}} - \eta b(\tilde{\boldsymbol{w}}^{\mathrm{T}}(t)P^{\mathrm{T}}P\tilde{\boldsymbol{w}}(t))\\
&\quad - \eta c(mn)^{\frac{1-\nu}{2}}(\tilde{\boldsymbol{w}}^{\mathrm{T}}(t)P^{\mathrm{T}}P\tilde{\boldsymbol{w}}(t))^{\frac{1+\nu}{2}} + \|\tilde{\boldsymbol{w}}(t)\|_2\cdot\sigma
\end{aligned}$$

$$\leq -\eta a(\lambda\|\tilde{\boldsymbol{w}}(t)\|_2^2)^{\frac{1+\mu}{2}} - \eta b\lambda\|\tilde{\boldsymbol{w}}(t)\|_2^2 - \eta c(mn)^{\frac{1-\nu}{2}}(\lambda\|\tilde{\boldsymbol{w}}(t)\|_2^2)^{\frac{1+\nu}{2}} + \|\tilde{\boldsymbol{w}}(t)\|_2\cdot\sigma$$
$$\leq -\eta a\lambda^{\frac{1+\mu}{2}}\|\tilde{\boldsymbol{w}}(t)\|_2^{1+\mu} + \|\tilde{\boldsymbol{w}}(t)\|_2\cdot\sigma$$
$$= -\|\tilde{\boldsymbol{w}}(t)\|_2(\eta a\lambda^{\frac{1+\mu}{2}}\|\tilde{\boldsymbol{w}}(t)\|_2^{\mu} - \sigma). \tag{9}$$

Then, according to the sign of $\eta a\lambda^{(1+\mu)/2}\|\tilde{\boldsymbol{w}}(t)\|_2^{\mu} - \sigma$, we make the following theoretical analysis.

1) If in the time interval $[t_0, t_1]$, $\eta a\lambda^{(1+\mu)/2}\|\tilde{\boldsymbol{w}}(t)\|_2^{\mu} - \sigma > 0$ holds, it follows from (9) that $\dot{\varpi}(t) < 0$, which indicates that $\varpi(t)$ tends to 0. That is to say, $X(t)$ tends to the theoretical solution X^* over time. Therefore, the solution error $\|\tilde{\boldsymbol{w}}(t)\|_2 = \|X(t) - X^*\|_{\mathrm{F}}$ will approach the upper bound $(\sigma/(\eta a\lambda^{(1+\mu)/2}))^{1/\mu}$ over time once it exceeds the upper bound;
2) For any time t, if $\eta a\lambda^{(1+\mu)/2}\|\tilde{\boldsymbol{w}}(t)\|_2^{\mu} - \sigma = 0$ holds, then $\|\tilde{\boldsymbol{w}}(t)\|_2 > 0$, it follows from (9) that $\dot{\varpi}(t) < 0$, which indicates that the solution error $\|\tilde{\boldsymbol{w}}(t)\|_2 = \|X(t) - X^*\|_{\mathrm{F}}$ continues to fall and $\|X(t) - X^*\|_{\mathrm{F}} < (\sigma/(\eta a\lambda^{(1+\mu)/2}))^{1/\mu}$ holds;
3) For any time instant t, if $\eta a\lambda^{(1+\mu)/2}\|\tilde{\boldsymbol{w}}(t)\|_2^{\mu} - \sigma < 0$ holds, it follows from (9) that $\dot{\varpi}(t) \leq c$, where c is a positive number. In this situation, we have $\dot{\varpi}(t) \leq 0$ or $0 < \dot{\varpi}(t) \leq c$. If $\dot{\varpi}(t) \leq 0$ still holds, then the solution error $\|\tilde{\boldsymbol{w}}(t)\|_2 = \|X(t) - X^*\|_{\mathrm{F}}$ continues to fall or keeps unchanged within the so-called ball $\|X(t) - X^*\|_{\mathrm{F}} = (\sigma/(\eta a\lambda^{(1+\mu)/2}))^{1/\mu}$; if $0 < \dot{\varpi}(t) \leq c$, then the solution error $\|\tilde{\boldsymbol{w}}(t)\|_2 = \|X(t) - X^*\|_{\mathrm{F}}$ will increase with time. However, it can never exceed the upper bound $(\sigma/(\eta a\lambda^{(1+\mu)/2}))^{1/\mu}$ since $\dot{\varpi}(t) \leq 0$ as analyzed above.

The proof is completed by summing up the above analysis. ■

It is noteworthy that according to the above analysis, the solution error $\|X(t) - X^*\|_{\mathrm{F}}$ approaches the upper bound $(\sigma/(\eta a\lambda^{(1+\mu)/2}))^{1/\mu}$ in an asymptotic way, which could be slow and unsatisfactory in practice [35]. Therefore, it is necessary to make a further analysis of this issue, which leads to the following results.

Theorem 3: In addition to Theorem 2, if GNN model (4) is disturbed by a dynamic bounded non-vanishing noise $R(t)$ satisfying $\|R(t)\|_{\mathrm{F}} \leq \sigma$ with $\sigma > 0$ being a constant. Then, under arbitrary initial condition $X(0)$, the solution error $\|X(t) - X^*\|_{\mathrm{F}}$ of GNN model (4) globally exponentially approaches and then stays within the upper bound $\left(\frac{\sigma}{\eta a\lambda^{(1+\mu)/2}}\right)^{1/\mu}$, or always stays within the upper bound $\left(\frac{\sigma}{\eta a\lambda^{(1+\mu)/2}}\right)^{1/\mu}$. Furthermore, the exponential convergence rate is $\eta b\lambda$, and the convergence time is at most:

$$t_{\mathrm{c}} = \frac{\mu\ln\|X(0) - X^*\|_{\mathrm{F}} + \ln\eta + \ln a + \frac{1+\mu}{2}\ln\lambda - \ln\sigma}{\mu\eta b\lambda} \tag{10}$$

Proof: For any time t, if the solution error $\|X(t) - X^*\|_{\mathrm{F}}$ is not less than the upper bound $(\sigma/(\eta a\lambda^{(1+\mu)/2}))^{1/\mu}$, it follow from (9) that

$$\dot{\varpi}(t) \leq -\eta a(\lambda\|\tilde{\boldsymbol{w}}(t)\|_2^2)^{\frac{1+\mu}{2}} - \eta b\lambda\|\tilde{\boldsymbol{w}}(t)\|_2^2 - \eta c(mn)^{\frac{1-\nu}{2}}(\lambda\|\tilde{\boldsymbol{w}}(t)\|_2^2)^{\frac{1+\nu}{2}} + \|\tilde{\boldsymbol{w}}(t)\|_2\cdot\sigma$$
$$\leq -\eta a\lambda^{\frac{1+\mu}{2}}\|\tilde{\boldsymbol{w}}(t)\|_2^{1+\mu} + \|\tilde{\boldsymbol{w}}(t)\|_2\cdot\sigma - \eta b\lambda\|\tilde{\boldsymbol{w}}(t)\|_2^2$$
$$= -\|\tilde{\boldsymbol{w}}(t)\|_2(\eta a\lambda^{\frac{1+\mu}{2}}\|\tilde{\boldsymbol{w}}(t)\|_2^{\mu} - \sigma) - 2\eta b\lambda\varpi(t)$$
$$\leq -2\eta b\lambda\varpi(t), \tag{11}$$

which leads to $\varpi(t) \leq \varpi(0)\exp(-2\eta b\lambda t)$. In view of $\varpi(t) = \|\tilde{\boldsymbol{w}}(t)\|_2^2/2$ and $\tilde{\boldsymbol{w}}(t) = \mathrm{vec}(X(t)) - \mathrm{vec}(X^*)$, we have $\|X(t) - X^*\|_{\mathrm{F}} \leq \|X(0) - X^*\|_{\mathrm{F}}\exp(-\eta b\lambda t)$, which indicates that the exponential convergence rate is $\eta b\lambda$. Let $\|X(0) - X^*\|_{\mathrm{F}}\exp(-\eta b\lambda t)$ equal the upper bound $(\sigma/(\eta a\lambda^{(1+\mu)/2}))^{1/\mu}$, the finite convergence time is thus derived as

$$t_{\mathrm{c}} = \frac{\mu\ln\|X(0) - X^*\|_{\mathrm{F}} + \ln\eta + \ln a + \frac{1+\mu}{2}\ln\lambda - \ln\sigma}{\mu\eta b\lambda}.$$

On the other hand, for any time t, if the solution error $\|X(t) - X^*\|_{\mathrm{F}}$ is less than the upper bound $(\sigma/(\eta a\lambda^{(1+\mu)/2}))^{1/\mu}$, according to the analysis presented in Theorem 2, it will always keep within the upper bound $(\sigma/(\eta a\lambda^{(1+\mu)/2}))^{1/\mu}$. The proof is completed. ■

C. CONSTANT NOISE

When $R(t)$ is a matrix-form constant noise, we have the following results regards the SSSE bound and the corresponding convergence time of the GNN model (4).

Theorem 4: For the Sylvester equation (1) with the unique theoretical solution X^*, if GNN model (4) is disturbed by a constant noise $R(t) = R$ satisfying $\|R(t)\|_{\mathrm{F}} \leq \delta$ with $\delta > 0$ being a constant. Then, under arbitrary initial condition $X(0)$, the SSSE of the GNN model (4) is given as

$$\lim_{t\to+\infty}\|X(t) - X^*\|_{\mathrm{F}} < \left(\frac{\delta}{\eta a\lambda^{\frac{1+\mu}{2}}}\right)^{1/\mu}, \tag{12}$$

where $\lambda > 0$ denotes the minimal eigenvalue of $P^{\mathrm{T}}P$ with P defined the same as that in Theorem 1. It follows from (12) that the SSSE approaches 0 as $\eta a \to +\infty$.

Proof: It can be generalized from the proof of Theorem 2. ■

Theorem 5: In addition to Theorem 4, if GNN model (4) is disturbed by a constant noise $R(t) = R$ satisfying $\|R(t)\|_{\mathrm{F}} \leq \delta$ with $\delta > 0$ being a constant. Then, under arbitrary initial condition $X(0)$, the solution error $\|X(t) - X^*\|_{\mathrm{F}}$ of GNN model (4) globally exponentially approaches and then stays within the upper bound $\left(\frac{\delta}{\eta a\lambda^{(1+\mu)/2}}\right)^{1/\mu}$, or always stays within the upper bound $\left(\frac{\delta}{\eta a\lambda^{(1+\mu)/2}}\right)^{1/\mu}$. Furthermore, the exponential convergence rate is $\eta b\lambda$, and the convergence time is at most:

$$t_{\mathrm{c}} = \frac{\mu\ln\|X(0) - X^*\|_{\mathrm{F}} + \ln\eta + \ln a + \frac{1+\mu}{2}\ln\lambda - \ln\delta}{\mu\eta b\lambda} \tag{13}$$

Proof: It can be generalized from the proof of Theorem 3. ■

III. SIMULATION VERIFICATIONS

In this section, to verify the above theoretical results, two illustrative examples are considered.

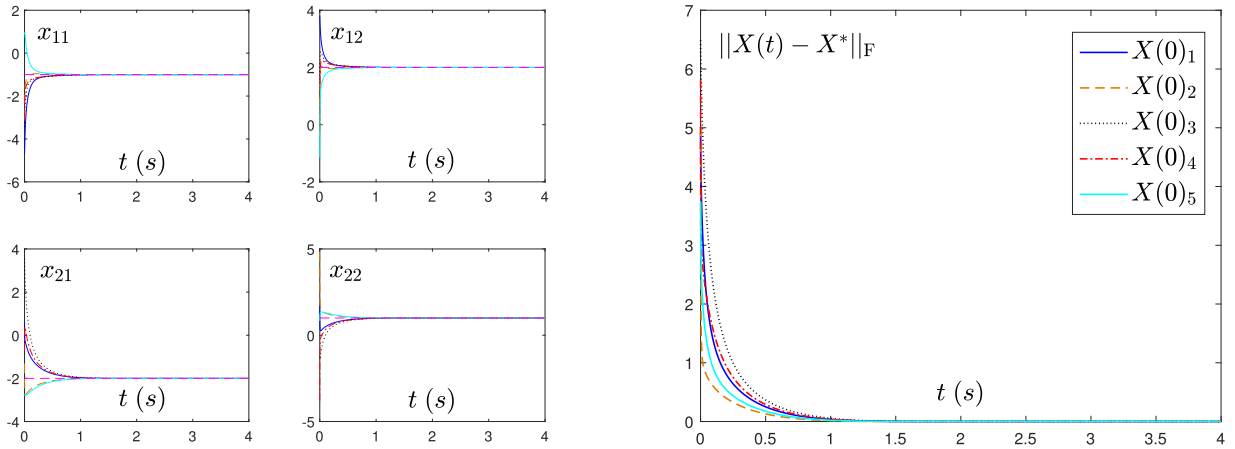

(a) Neural state $X(t)$ (b) Solution error $\|X(t) - X^*\|_{\mathrm{F}}$

FIGURE 1. Neural state $X(t)$ and solution error $\|X(t) - X^*\|_{\mathrm{F}}$ of GNN model (4) disturbed by a dynamic bounded vanishing noise.

A. EXAMPLE 1

We firstly take into consideration the same example illustrated in [26], of which the coefficient matrices are as follows:

$$C = \begin{bmatrix} 2 & 1 \\ -1 & 1 \end{bmatrix}, \quad D = \begin{bmatrix} 2 & 3 \\ 4 & 5 \end{bmatrix}, \quad F = \begin{bmatrix} 10 & 2 \\ 1 & 0 \end{bmatrix}. \quad (14)$$

The exact solution is $X^* = [-1, 2; -2, 1]$. In addition, it is easy to obtain the minimal eigenvalue of matrix $P^{\mathrm{T}}P$ as $\lambda = 2.3020$. Three types of noises will be considered for the noise-polluted GNN model (4), and the following five randomly generated matrices are used as the initial value $X(0)$:

$$X(0)_1 = \begin{bmatrix} -4.6740 & 3.8187 \\ 0.6120 & 1.6918 \end{bmatrix},$$
$$X(0)_2 = \begin{bmatrix} -3.0957 & -0.3927 \\ -1.3108 & 4.8164 \end{bmatrix},$$
$$X(0)_3 = \begin{bmatrix} -3.4360 & 1.4476 \\ 3.5552 & -1.2373 \end{bmatrix},$$
$$X(0)_4 = \begin{bmatrix} -3.0908 & -0.1798 \\ -0.7175 & -3.7939 \end{bmatrix},$$
$$X(0)_5 = \begin{bmatrix} 0.8951 & -1.1538 \\ -2.7381 & 0.8299 \end{bmatrix}.$$

In the following simulations, the parameters are set as $\eta = a = b = c = 1, \mu = 0.8, \nu = 2$. Firstly, we consider the situation where $R(t)$ is a dynamic bounded vanishing noise, i.e., $R(t) = \epsilon(X(t) - X^*)$ with $\epsilon = 2.3 < \lambda\eta b$. The convergence curves of neural state $X(t)$ and solution error $\|X(t) - X^*\|_{\mathrm{F}}$ are shown in Fig. 1. It can be concluded from this figure that $X(t)$, starting from the above five different initial values, is convergent to the exact solution X^* within $T_{\max} = 2.9353$ s computed by the formula (5).

Secondly, we consider the situation where $R(t)$ is the following dynamic bounded non-vanishing noise

$$R(t) = \sqrt{2}\begin{bmatrix} \sin(2t) & \cos(2t) \\ \cos(2t) & \sin(2t) \end{bmatrix}. \quad (15)$$

TABLE 1. Upper bound of time for the solution error of GNN model (4) approaching the upper bound under five different initial values when disturbed by the dynamic bounded non-vanishing noise (15).

Initial value	$X(0)_1$	$X(0)_2$	$X(0)_3$	$X(0)_4$	$X(0)_5$
t_{c} (s)	0.7223	0.7316	0.8435	0.7954	0.6060

Simulation results are shown in Fig. 2. It can be seen that the solution error $\|X(t) - X^*\|_{\mathrm{F}}$ approaches the upper bound within the time presented in Table 1 and then stays within the upper bound.

Finally, we consider the situation where $R(t)$ is a constant noise with each element being 1. Simulation results are shown in Fig. 3, from which we can draw the same conclusion as the second situation.

B. EXAMPLE 2

Let us take into consideration another Sylvester equation:

$$C = \begin{bmatrix} 2.6136 & 0.1955 & 0.0082 \\ 0.1931 & 3.5120 & 1.1712 \\ 1.1734 & 1.7351 & 3.7144 \end{bmatrix},$$
$$D = \begin{bmatrix} 3.3480 & 2.1092 & 2.9538 \\ 4.5623 & 3.1340 & 2.9342 \\ 0.2822 & 3.8121 & 1.7524 \end{bmatrix},$$
$$F = \begin{bmatrix} 5.9603 & 1.2454 & 1.5647 \\ 4.6199 & 2.1198 & 1.9252 \\ 5.2646 & 0.3684 & 2.5287 \end{bmatrix},$$
$$X^* = \begin{bmatrix} -0.6290 & 1.3900 & 0.5481 \\ 0.3390 & 1.1834 & 0.9103 \\ 0.9409 & 1.1522 & 0.7180 \end{bmatrix}, \quad (16)$$

of which the minimal eigenvalue of matrix $P^{\mathrm{T}}P$ can be obtained as $\lambda = 2.6569$, and the following five randomly-generated matrices are used as the initial value $X(0)$:

$$X(0)_1 = \begin{bmatrix} -1.7740 & 1.2096 & -0.9995 \\ -1.8798 & 1.5877 & -0.3560 \\ -0.0169 & -2.5120 & 1.0187 \end{bmatrix},$$

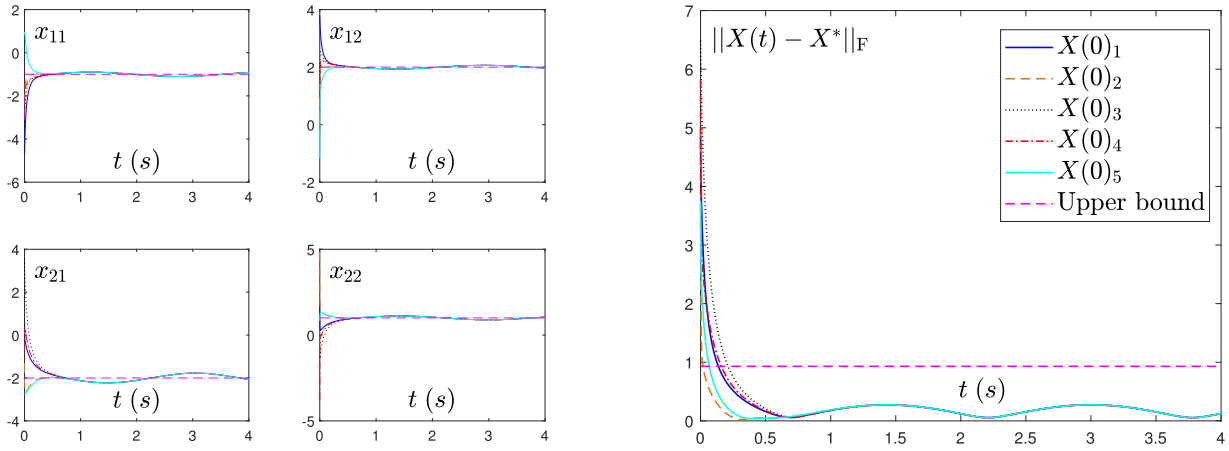

(a) Neural state $X(t)$ (b) Solution error $\|X(t) - X^*\|_{\mathrm{F}}$

FIGURE 2. Neural state $X(t)$ and solution error $\|X(t) - X^*\|_{\mathrm{F}}$ of GNN model (4) disturbed by a dynamic bounded non-vanishing noise.

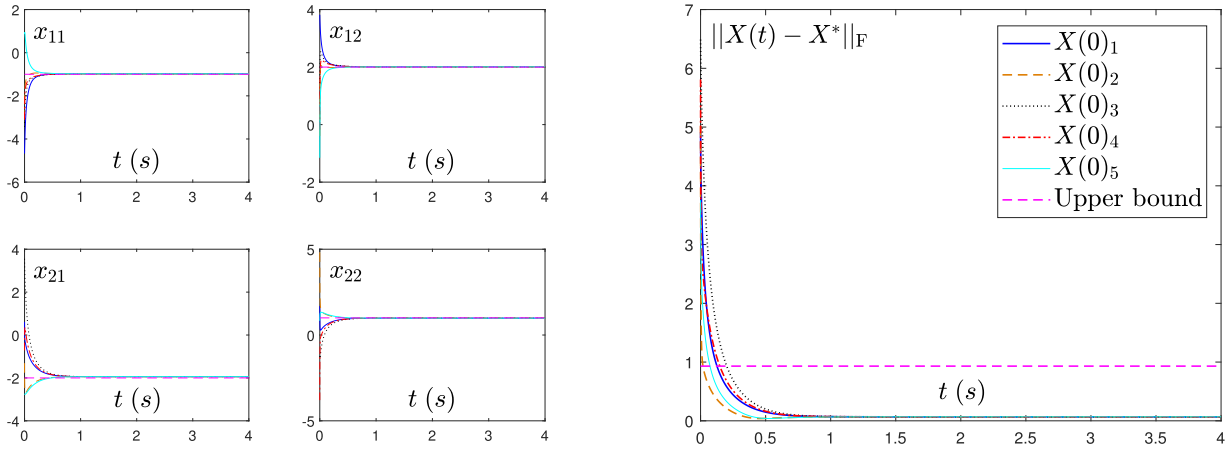

(a) Neural state $X(t)$ (b) Solution error $\|X(t) - X^*\|_{\mathrm{F}}$

FIGURE 3. Neural state $X(t)$ and solution error $\|X(t) - X^*\|_{\mathrm{F}}$ of GNN model (4) disturbed by a constant noise.

$$X(0)_2 = \begin{bmatrix} 1.6713 & -0.7689 & -1.3119 \\ 2.7831 & -0.0627 & -0.5854 \\ -2.7769 & -2.9727 & 0.3185 \end{bmatrix},$$

$$X(0)_3 = \begin{bmatrix} -2.0486 & 2.7132 & -1.1537 \\ 0.1794 & -2.3786 & 2.4635 \\ 0.4846 & 0.5822 & -1.7432 \end{bmatrix},$$

$$X(0)_4 = \begin{bmatrix} 2.9474 & -0.1606 & -1.1620 \\ 1.6377 & -2.3293 & -0.1148 \\ 1.4724 & -2.1985 & 2.1044 \end{bmatrix},$$

$$X(0)_5 = \begin{bmatrix} -2.2843 & -1.7610 & 0.2064 \\ 0.6878 & -0.4898 & 2.0148 \\ 0.6849 & 0.1824 & -2.1099 \end{bmatrix}.$$

In the following simulation, the parameters of the GNN model (4) are set the same as that of example 1. Three different noises, i.e.,

$$R(t) = 2.65(X(t) - X^*), \tag{17}$$

$$R(t) = \begin{bmatrix} \sin(3t) & -\cos(3t) & \sin(3t) \\ \cos(3t) & \sin(3t) & -\cos(3t) \\ -\cos(3t) & 0 & -\sin(3t) \end{bmatrix}, \tag{18}$$

TABLE 2. Upper bound of time for the solution error of GNN model (4) approaching the upper bound under five different initial values when disturbed by the dynamic bounded non-vanishing noise (18).

Initial value	$X(0)_1$	$X(0)_2$	$X(0)_3$	$X(0)_4$	$X(0)_5$
t_c (s)	0.6924	0.8389	0.7173	0.8107	0.7003

$$R(t) = \begin{bmatrix} 1 & 1 & 1 \\ 1 & 1 & 1 \\ 1 & 1 & 1 \end{bmatrix}, \tag{19}$$

are investigated. The simulation results are presented in Fig. 4 and Table 2, which are consistent with theoretical analyses.

In short, the above simulation results verify the theoretical analyses presented in Section II.

IV. ROBOTIC APPLICATION

In this section, we conduct a robot path tracking example with the aid of the GNN model (4). The task of the used four-link planar robot arm is to track an epicycloid path. The solution

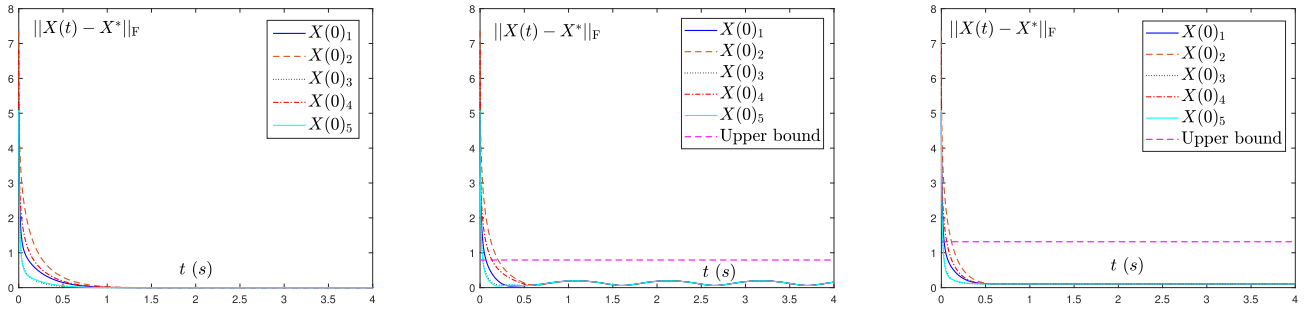

(a) Dynamic bounded vanishing noise (17) (b) Dynamic bounded non-vanishing noise (18) (c) Constant noise (19)

FIGURE 4. Solution error $\|X(t) - X^*\|_F$ of GNN model (4) disturbed by three kinds of noises for example 2.

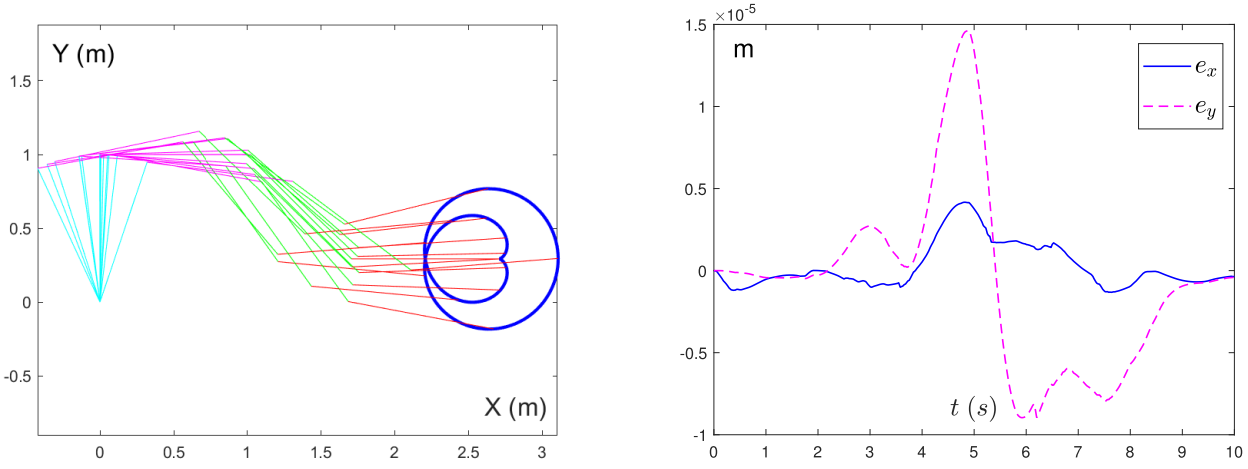

(a) Movement tracks (b) End-effector positioning errors

FIGURE 5. Movement tracks and end-effector positioning errors of the planar four-link robot arm.

of the minimum velocity norm scheme with feedback can be written as [18], [36]

$$\dot{\boldsymbol{\theta}} = J^{+}(\dot{\boldsymbol{r}}_e + \kappa(\boldsymbol{r}_e - \varphi(\boldsymbol{\theta}))), \tag{20}$$

where vectors $\boldsymbol{\theta} \in \mathbb{R}^4$ and $\dot{\boldsymbol{\theta}} \in \mathbb{R}^4$ are the joint and joint-velocity of the planar four-link robot arm, $\varphi(\cdot)$ is the nonlinear mapping function determined by the structure and parameters of the planar four-link robot arm, $J^{+} \in \mathbb{R}^{4\times 2}$ and $\dot{\boldsymbol{r}}_e$ are respectively used to indicate the pseudoinverse of the Jacobian matrix J and the time derivative of the expected end-effector path $\boldsymbol{r}_e$. In addition, $\kappa > 0$ indicates the feedback factor.

In the simulation, the parameters of GNN model (4) and the planar four-link robot manipulator are set as $\eta = 5 \times 10^4, a = b = c = 1, \mu = 0.8, \nu = 2$, every entry of the noise matrix $R(t)$ is $2\sin(t)$, the length of every link is $l_i = 1$ m $(i = 1, 2, 3, 4)$, and the initial value of $\boldsymbol{\theta}(t)$ is $\boldsymbol{\theta}(0) = [\pi/2; -\pi/2; -\pi/4; \pi/4]$ rad. Fig. 5 illustrates the simulation results. Given that the maximal positioning error of the end-effector is of order 10^{-5}m, one can conclude that the path-tracking task has been achieved well.

V. CONCLUSION

In this paper, the robustness against three kinds of noises of the fixed-time convergent GNN model (4) for solving the Sylvester equation has been investigated. Specifically, if disturbed by a dynamic bounded vanishing noise, the GNN model (4) can still achieve fixed-time convergence, and if disturbed by a dynamic bounded non-vanishing or constant noise, an SSSE exists and has a bound. Furthermore, the convergence time of fixed-time convergence, the SSSE bound, and the finite time and exponential convergence rate for the solution error approaching the bound have been estimated through theoretical analyses. Computer simulation results have verified these facts. In addition, an example of path tracking of redundant robot arms has also been provided to show the feasibility and efficacy of the GNN model (4) to robotic applications.

REFERENCES

[1] S. G. Shafiei and M. Hajarian, "Developing Kaczmarz method for solving Sylvester matrix equations," *J. Franklin Inst.*, vol. 359, no. 16, pp. 8991–9005, Nov. 2022.

[2] L. Ding, L. Xiao, K. Zhou, Y. Lan, Y. Zhang, and J. Li, "An improved complex-valued recurrent neural network model for time-varying complex-valued Sylvester equation," *IEEE Access*, vol. 7, pp. 19291–19302, 2019.

[3] L. Xiao, "A finite-time recurrent neural network for solving online time-varying Sylvester matrix equation based on a new evolution formula," *Nonlinear Dyn.*, vol. 90, no. 3, pp. 1581–1591, Nov. 2017.
[4] J. Jin, L. Xiao, M. Lu, and J. Li, "Design and analysis of two FTRNN models with application to time-varying Sylvester equation," *IEEE Access*, vol. 7, pp. 58945–58950, 2019.
[5] L. Xiao and Y. He, "A noise-suppression ZNN model with new variable parameter for dynamic Sylvester equation," *IEEE Trans. Ind. Informat.*, vol. 17, no. 11, pp. 7513–7522, Nov. 2021.
[6] Z. Jian, L. Xiao, K. Li, Q. Zuo, and Y. Zhang, "Adaptive coefficient designs for nonlinear activation function and its application to zeroing neural network for solving time-varying Sylvester equation," *J. Franklin Inst.*, vol. 357, no. 14, pp. 9909–9929, Sep. 2020.
[7] L. Xiao, Y. Zhang, J. Dai, J. Li, and W. Li, "New noise-tolerant ZNN models with predefined-time convergence for time-variant Sylvester equation solving," *IEEE Trans. Syst., Man, Cybern., Syst.*, vol. 51, no. 6, pp. 3629–3640, Jun. 2021.
[8] Y. Qi, L. Jin, H. Li, Y. Li, and M. Liu, "Discrete computational neural dynamics models for solving time-dependent Sylvester equation with applications to robotics and MIMO systems," *IEEE Trans. Ind. Informat.*, vol. 16, no. 10, pp. 6231–6241, Oct. 2020.
[9] Y. Lei, J. Luo, T. Chen, L. Ding, B. Liao, G. Xia, and Z. Dai, "Nonlinearly activated IEZNN model for solving time-varying Sylvester equation," *IEEE Access*, vol. 10, pp. 121520–121530, 2022.
[10] K. Li, C. Jiang, X. Xiao, H. Huang, Y. Li, and J. Yan, "Residual error feedback zeroing neural network for solving time-varying Sylvester equation," *IEEE Access*, vol. 10, pp. 2860–2868, 2022.
[11] R. H. Bartels and G. W. Stewart, "Solution of the matrix equation AX + XB = C," *Commun. ACM*, vol. 15, no. 9, pp. 820–826, 1972.
[12] R. Zhou, X. Wang, and X.-B. Tang, "Preconditioned positive-definite and skew-Hermitian splitting iteration methods for continuous Sylvester equations $AX+XB=C$," *East Asian J. Appl. Math.*, vol. 7, no. 1, pp. 55–69, Feb. 2017.
[13] Z. Chen and X. Chen, "Modification on the convergence results of the Sylvester matrix equation $AX + XB = C$," *J. Franklin Inst.*, vol. 359, no. 7, pp. 3126–3147, 2022.
[14] F. Ding and T. Chen, "Gradient based iterative algorithms for solving a class of matrix equations," *IEEE Trans. Autom. Control*, vol. 50, no. 8, pp. 1216–1221, Aug. 2005.
[15] K. Chen, "Improved neural dynamics for online Sylvester equations solving," *Inf. Process. Lett.*, vol. 116, no. 7, pp. 455–459, Jul. 2016.
[16] D. Guo, C. Yi, and Y. Zhang, "Zhang neural network versus gradient-based neural network for time-varying linear matrix equation solving," *Neurocomputing*, vol. 74, no. 17, pp. 3708–3712, Oct. 2011.
[17] L. Jin, S. Li, L. Xiao, R. Lu, and B. Liao, "Cooperative motion generation in a distributed network of redundant robot manipulators with noises," *IEEE Trans. Syst., Man, Cybern., Syst.*, vol. 48, no. 10, pp. 1715–1724, Oct. 2018.
[18] Z. Tan, Y. Hu, L. Xiao, and K. Chen, "Robustness analysis and robotic application of combined function activated RNN for time-varying matrix pseudo inversion," *IEEE Access*, vol. 7, pp. 33434–33440, 2019.
[19] L. Xiao, Z. Zhang, and S. Li, "Solving time-varying system of nonlinear equations by finite-time recurrent neural networks with application to motion tracking of robot manipulators," *IEEE Trans. Syst., Man, Cybern., Syst.*, vol. 49, no. 11, pp. 2210–2220, Nov. 2019.
[20] Z. Tang, N. Tan, and Y. Zhang, "Velocity-layer Zhang equivalency for time-varying joint limits avoidance of redundant robot manipulator," *IET Control Theory Appl.*, vol. 16, no. 18, pp. 1909–1921, Dec. 2022.
[21] Z. Zhang, T. Fu, Z. Yan, L. Jin, L. Xiao, Y. Sun, Z. Yu, and Y. Li, "A varying-parameter convergent-differential neural network for solving joint-angular-drift problems of redundant robot manipulators," *IEEE/ASME Trans. Mechatronics*, vol. 23, no. 2, pp. 679–689, Apr. 2018.
[22] Z. Tan, W. Li, L. Xiao, and Y. Hu, "New varying-parameter ZNN models with finite-time convergence and noise suppression for time-varying matrix Moore–Penrose inversion," *IEEE Trans. Neural Netw. Learn. Syst.*, vol. 31, no. 8, pp. 2980–2992, Aug. 2020.
[23] H. Lu, L. Jin, X. Luo, B. Liao, D. Guo, and L. Xiao, "RNN for solving perturbed time-varying underdetermined linear system with double bound limits on residual errors and state variables," *IEEE Trans. Ind. Informat.*, vol. 15, no. 11, pp. 5931–5942, Nov. 2019.
[24] Y. Zhang, B. Qiu, B. Liao, and Z. Yang, "Control of pendulum tracking (including swinging up) of IPC system using zeroing-gradient method," *Nonlinear Dyn.*, vol. 89, no. 1, pp. 1–25, Jul. 2017.
[25] W. Li, L. Han, X. Xiao, B. Liao, and C. Peng, "A gradient-based neural network accelerated for vision-based control of an RCM-constrained surgical endoscope robot," *Neural Comput. Appl.*, vol. 34, no. 2, pp. 1329–1343, Jan. 2022.
[26] Z. Tan, "Fixed-time convergent gradient neural network for solving online Sylvester equation," *Mathematics*, vol. 10, no. 17, p. 3090, Aug. 2022, doi: 10.3390/MATH10173090.
[27] Y. Zhang, S. Li, J. Weng, and B. Liao, "GNN model for time-varying matrix inversion with robust finite-time convergence," *IEEE Trans. Neural Netw. Learn. Syst.*, early access, May 24, 2022, doi: 10.1109/TNNLS.2022.3175899.
[28] L. Xiao, B. Liao, J. Luo, and L. Ding, "A convergence-enhanced gradient neural network for solving Sylvester equation," in *Proc. 36th Chin. Control Conf.*, 2017, pp. 3910–3913.
[29] W. Li, B. Liao, L. Xiao, and R. Lu, "A recurrent neural network with predefined-time convergence and improved noise tolerance for dynamic matrix square root finding," *Neurocomputing*, vol. 337, pp. 262–273, Apr. 2019.
[30] K. Chen and C. Yi, "Robustness analysis of a hybrid of recursive neural dynamics for online matrix inversion," *Appl. Math. Comput.*, vol. 273, pp. 969–975, Jan. 2016.
[31] C. Chen, L. Li, H. Peng, and Y. Yang, "Fixed-time synchronization of inertial memristor-based neural networks with discrete delay," *Neural Netw.*, vol. 109, pp. 81–89, Jan. 2019.
[32] G. Hardy, J. Littlewood, and G. Polya, *Inequalities*. Cambridge, U.K.: Cambridge Univ. Press, 1952.
[33] Z. Tan, Y. Hu, and K. Chen, "On the investigation of activation functions in gradient neural network for online solving linear matrix equation," *Neurocomputing*, vol. 413, pp. 185–192, Nov. 2020.
[34] F. Ding and H. Zhang, "Gradient-based iterative algorithm for a class of the coupled matrix equations related to control systems," *IET Control Theory Appl.*, vol. 8, no. 15, pp. 1588–1595, Oct. 2014.
[35] Y. Zhang, K. Chen, and H.-Z. Tan, "Performance analysis of gradient neural network exploited for online time-varying matrix inversion," *IEEE Trans. Autom. Control*, vol. 54, no. 8, pp. 1940–1945, Aug. 2009.
[36] D. Guo and Y. Zhang, "Li-function activated ZNN with finite-time convergence applied to redundant-manipulator kinematic control via time-varying Jacobian matrix pseudoinversion," *Appl. Soft Comput.*, vol. 24, pp. 158–168, Nov. 2014.

ZHIGUO TAN received the Ph.D. degree in control theory and control engineering from the South China University of Technology, Guangzhou, China, in 2019. His research interests include neural networks, nonlinear systems, robotics, and intelligent computing.

ZHENLUN YANG received the Ph.D. degree from the South China University of Technology, in 2016. He is currently an Associate Professor with the School of Information Engineering, Guangzhou Panyu Polytechnic, Guangzhou, China. His current research interests include neural networks, evolutionary computing, and the Internet of Things.